Application of a single step temporal imaging of magnetic induction tomography for metal flow visualization

Manuchehr Soleimani[1], Andy Adler[2], Tao Dai[2] , A J Peyton[3]

[1.] Department of Electronic & Electrical Engineering, University of Bath, Bath, UK, Email: m.soleimani@bath.ac.uk
[2.] Systems and Computer Engineering, Carleton University, Ottawa, Canada
[3.] School of electrical Engineering and electronics, University of Manchester, Manchester, UK

Abstract. Magnetic induction tomography (MIT) is a new technique to image the electromagnetic properties of an object by mutual induction data of pairs of excitation and sensing coils. MIT has potential in visualization of metal flow for continuous casting mainly because of its potential to deliver images with high temporal resolution.

A dynamic magnetic induction imaging technique is developed with the aid of a novel direct temporal imaging method. This paper proposes a new approach, which directly accounts for correlations between images in successive data frames. The forward problem in MIT is a general eddy current problem and is solved by an edge finite element method. The inverse problem is treated as a dynamical inverse problem, and the conductivity distribution is estimated with the aid of the direct temporal imaging method. Experimental tests illustrate the performances in the sense of spatio-temporal resolution using the real metal flow in continuous casting. Results are compared with reconstruction algorithms based on independent frames.

Index Terms: Electro-magnetic induction tomography, conductivity mapping, inverse problem, dynamic imaging, direct temporal imaging.

1. INTRODUCTION

Magnetic induction tomography (MIT) is a new modality for medical, industrial and geophysical imaging [1], [3], [10]. The measurement data are the mutual inductances between pairs of coils. The contact-less nature of this type of tomography makes the technique of interest for non-invasive and non-intrusive applications. The technique operates as follows. Passing an alternating current through the excitation coil(s) produces a primary magnetic field. When this magnetic field interacts with either a conductive and/or a magnetic object, a secondary magnetic field is created. The sensing coils can then detect this secondary field. As the secondary field depends on the materials present, the measured induced voltage is a non-linear function of their electrical properties, e.g., conductivity [11] and permeability [12].

MIT has a potential to be used in many industrial applications [1]. This paper concentrates on imaging the molten steel flow, especially the on-line flow visualization approach.

Online flow visualization often requires very fast tomography data. Among non-invasive imaging techniques, MIT has a much higher temporal resolution than others such as CT, etc. This makes MIT one of the best candidate, which is capable of long term monitering of fast-varying, dynamic flow. However, the spatial resolution of MIT is low due to facts as: the measurement being effectively insensitive to deep internal conductivity changes; MIT reconstruction is severely ill-conditioned. In order to solve the ill-conditionness of MIT, *a priori* knowledge of true images are necessary for regularization techniques. *a*

priori knowledge is interpreted as a regularized matrix which represents the underlying image probability distribution in Bayesian's theory .

Static MIT imaging techniques uses a single set of measurements for one image. Even if the measurements are fast compared to the changes in material properties, the static methods do not take into account the correlation between images of different frames.

In order to enhance the temporal resolution a novel dynamic imaging techniques have been proposed. Most previous work in similar applications is using Kalman filters [4], [5] for situations where the conductivity distribution changes rapidly in the electrical tomography applications, [6], [7], [15]. This paper evaluates the new temporal imaging method using experimental test example from continuous casting.

2 THEORETICAL METHOD

A. *Forward problem in MIT*

MIT is working based on eddy current concept [11]. By ignoring the wave propagation effect in Maxwell's equation and by taking $E = -i\omega A^*$, $A^* - A$ formulation can be used to solve the forward problem in MIT [11]

$$\nabla \times (\frac{1}{\mu} \nabla \times A^*) + i\omega\sigma A^* = J_0 \qquad (1)$$

where J_0 is the current density in the excitation coil, μ is the permeability, σ. is the conductivity, A is the magnetic vector potential in free space and A^* is the magnetic vector potential in the conducting region, which includes the gradient of scalar field.

The edge FEM has some advantages over other conventional nodal FEM and has been implemented for solving the forward problem in MIT [11]. The degrees of freedom are

the line integrals of the vector quantities along the edges of a mesh. The interface condition between two elements is satisfied, so that the results from edge based finite elements are more accurate than those from nodal elements. An incomplete Cholesky Conjugate Gradient (ICCG) approach has been applied to solve the linear system of equations arising form the edge FEM. Considering that ϕ_i is the nodal scalar basis function, in an edge FEM on a tetrahedral mesh a vector field is represented using a basis of vector valued functions, where N_{ij} associated with the edge between nodes i, j.

$$Nij = \phi_i \nabla \phi_j - \phi_j \nabla \phi_i \tag{2}$$

Galerkin's approximation using edge element basis functions yields

$$\int_{\Omega} (\nabla \times N \cdot \frac{1}{\mu} \nabla \times A^*)\, dx^3 + \int_{\Omega_e} (i\omega\sigma N \cdot A^*)\, dx^3 = \int_{\Omega_c} (N \cdot J_0)\, dx^3 \tag{3}$$

where N is any linear combination of edge basis functions, Ω is the entire region, Ω_e the eddy current region, and Ω_c the current source region.

The current source can be defined by the electric vector potential $J_0 = \nabla \times T_0$, which clearly guarantees that $\nabla \cdot J_0 = 0$. This is important for the convergence of the linear system of equations arising from edge FEM [11], [12], [13].

With the $A^* - A$ formulation and using edge FEM, the sensitivity to change in conductivity of the conducting area can be calculated using the dot product of two electric fields [2],[8],[12],[13]. Considering $E = -i\omega A^*$, where the integral becomes the inner product of A fields, the Jacobian can be calculated by performing the integration for a chosen basis for the conductivity perturbation $\delta\sigma$. Using the matrix of shape

function in each element $\{N_e\}$ the potential A^* inside each element can be expressed as $A^* = \{N_e\} \cdot \{A_e\}$, where $\{A_e\}$ is defined along edges. The sensitivity term for each element is

$$S = \frac{\partial V_{ij}}{\partial \sigma_m} = -\frac{\omega^2}{I_i I_j} \{A_e^i\} \left(\int_{\Omega_m} \{N_e\} \cdot \{N_e\}^T dx^3 \right) \{A_e^j\}^T \tag{4}$$

This expression gives the sensitivity of the pair of coils i, j with an induced voltage to an element. Here, Ω_m is the volume of element number m, and I_i and I_j are excitation currents into the coils.

B. Static imaging

In image reconstruction linear algorithms are considered, the linear model $z = Jx + n$. The linearized inverse problem is based on Tikhonov regularization, which is to seek the minimum of

$$\|\mathbf{z} - \mathbf{J}\mathbf{x}\|^2 + \lambda \|\mathbf{x}\|^2 \tag{5}$$

where **x** is the image pixel vector, which is an image of change in conductivity, **z** is the measurement vector, which is voltage differences between simulated induced voltages from the forward solution and the measured ones, n is the noise in measured data, **J** is the sensitivity matrix (Jacobian matrix), and λ is a regularization parameter. Note that $\|b\| = \sqrt{\sum_k b_k^2}$. The minimum of equation (5) is found to be

$$\mathbf{x} = (\mathbf{J}^T \mathbf{J} + \lambda \mathbf{I})^{-1} \mathbf{J}^T \mathbf{z} \tag{6}$$

where **I** is an identity matrix, λ is regularization parameter (hyperparameter). This is a single step Gauss-Newton (GN) solution for the static inverse problem. In this single-step algorithm, sensitivity matrix **J** was obtained with a direct measurement method [9], [14].

C: Temporal imaging

Instead of calculating an image based on the sequence of past frames, we propose a temporal image reconstruction algorithm which uses a set of data frames nearby in time [12]. The data frame sequence is treated as a single inverse problem, with regularization prior to account for both spatial and temporal correlations between image elements. Given a vertically concatenated sequence of measurements frames $\tilde{\mathbf{z}} = [\mathbf{z}_{-d}; \ldots; \mathbf{z}_0; \ldots; \mathbf{z}_d]$ and the corresponding concatenated images $\tilde{\mathbf{x}} = [\mathbf{x}_{-d}; \ldots; \mathbf{x}_0; \ldots; \mathbf{x}_d]$, the direct temporal forward model $z = Jx + n$ is rewritten as

$$\begin{bmatrix} \mathbf{z}_{-d} \\ \vdots \\ \mathbf{z}_0 \\ \vdots \\ \mathbf{z}_d \end{bmatrix} = \begin{bmatrix} \mathbf{J} & \cdots & 0 \\ \ddots & & \\ \vdots & \mathbf{J} & \vdots \\ & \ddots & \\ 0 & \cdots & \mathbf{J} \end{bmatrix} \begin{bmatrix} \mathbf{x}_{-d} \\ \vdots \\ \mathbf{x}_0 \\ \vdots \\ \mathbf{x}_d \end{bmatrix} + \begin{bmatrix} \mathbf{n}_{-d} \\ \vdots \\ \mathbf{n}_0 \\ \vdots \\ \mathbf{n}_d \end{bmatrix} \tag{7}$$

and also as

$$\tilde{\mathbf{z}} = \tilde{\mathbf{J}}\tilde{\mathbf{x}} + \tilde{\mathbf{n}} \tag{8}$$

where $\tilde{\mathbf{n}} = [\mathbf{n}_{-d}; \ldots; \mathbf{n}_0; \ldots; \mathbf{n}_d]$ is the noise in measured data. We assume $\mathbf{J}$ to be constant, although this formulation could be modified to account for a time varying $\mathbf{J}$. Based on this approximation $\tilde{\mathbf{J}} = \mathbf{I} \otimes \mathbf{J}$, where the identity $\mathbf{I}$ has size 2d+1, and $\otimes$ is the Kronecker product.

The correlation of corresponding elements between adjacent frames (delay t=1) can be evaluated by an inter-frame correlation γ, which has value between 0 (independent) and 1 (fully dependent). As frames become separated in time, the inter-frame correlation decreases; for an inter-frame separation t, the inter-frame correlation is γ^t. Frames with

large time lag, |t|>d, can be considered independent. Image reconstruction is then defined in terms of minimizing the augmented expression:

$$\left\| \begin{bmatrix} \mathbf{z}_{-d} \\ \vdots \\ \mathbf{z}_0 \\ \vdots \\ \mathbf{z}_d \end{bmatrix} - \begin{bmatrix} \mathbf{J} & & \cdots & & 0 \\ & \ddots & & & \\ \vdots & & \mathbf{J} & & \vdots \\ & & & \ddots & \\ 0 & & \cdots & & \mathbf{J} \end{bmatrix} \begin{bmatrix} \mathbf{x}_{-d} \\ \vdots \\ \mathbf{x}_0 \\ \vdots \\ \mathbf{x}_d \end{bmatrix} \right\|_{\tilde{\mathbf{W}}}^2 + \lambda^2 \left\| \begin{bmatrix} \mathbf{x}_{-d} \\ \vdots \\ \mathbf{x}_0 \\ \vdots \\ \mathbf{x}_d \end{bmatrix} \right\|_{\tilde{\mathbf{R}}}^2 \tag{9}$$

and the inversion can be written as

$$\tilde{\mathbf{B}} = \tilde{\mathbf{R}}^{-1}\tilde{\mathbf{J}}^T(\tilde{\mathbf{J}}\tilde{\mathbf{R}}^{-1}\tilde{\mathbf{J}}^T + \lambda^2\tilde{\mathbf{W}}^{-1})^{-1} \tag{10}$$

where $\tilde{\mathbf{W}} = \mathbf{I} \otimes \mathbf{W}$. $\tilde{\mathbf{W}}$ is diagonal since measurement noise is uncorrelated between frames. $\tilde{\mathbf{R}} = \mathbf{\Gamma}^{-1} \otimes \mathbf{R}$ where $\mathbf{\Gamma}$ is the temporal weight matrix of an image sequence $\tilde{\mathbf{x}}$ and is defined to have the form as

$$\mathbf{\Gamma} = \begin{bmatrix} 1 & \gamma & \cdots & \gamma^{2d-1} & \gamma^{2d} \\ \gamma & 1 & \cdots & \gamma^{2d-2} & \gamma^{2d-1} \\ \vdots & \vdots & \ddots & \vdots & \vdots \\ \gamma^{2d-1} & \gamma^{2d-2} & \cdots & 1 & \gamma \\ \gamma^{2d} & \gamma^{2d-1} & \cdots & \gamma & 1 \end{bmatrix} \tag{11}$$

From (10) and (11),

$$\tilde{\mathbf{B}} = \left[\mathbf{\Gamma} \otimes \left(\mathbf{P}\mathbf{J}^T\right)\right]\left[\mathbf{\Gamma} \otimes \left(\mathbf{J}\mathbf{P}\mathbf{J}^T\right) + \lambda^2(\mathbf{I} \otimes \mathbf{V})\right]^{-1} \tag{12}$$

(6) is rewritten as

$$\begin{bmatrix} \hat{\mathbf{x}}_{-d} \\ \vdots \\ \hat{\mathbf{x}}_0 \\ \vdots \\ \hat{\mathbf{x}}_d \end{bmatrix} = \tilde{\mathbf{B}}\tilde{\mathbf{y}} \tag{13}$$

Although this estimate is an augmented image sequence, we are typically only interested in the current image $\hat{\mathbf{x}}_0$. It is calculated by $\hat{\mathbf{x}}_0 = \tilde{\mathbf{B}}_0 \tilde{\mathbf{y}}$ where $\tilde{\mathbf{B}}_0$ is the rows $n_M d+1 \ldots n_M(d+1)$ of $\tilde{\mathbf{B}}$.

3 METHOD – DATA

A. MIT system

In this study an MIT sensor as shown in Figure 1 is used to generate data for image reconstruction [9]. A system consists of sensor array, data acquisition instrumentation and a PC. The sensor array consists of 8 coils for excitation and detection. The inner diameter of the coils is 4 cm, the outer diameter is 5 cm and the length is 2 cm. The coils are arranged in a circular ring surrounding an object to be imaged. The distance between the centres of two opposite coils is 16 cm. The excitation frequency is 5kHZ.

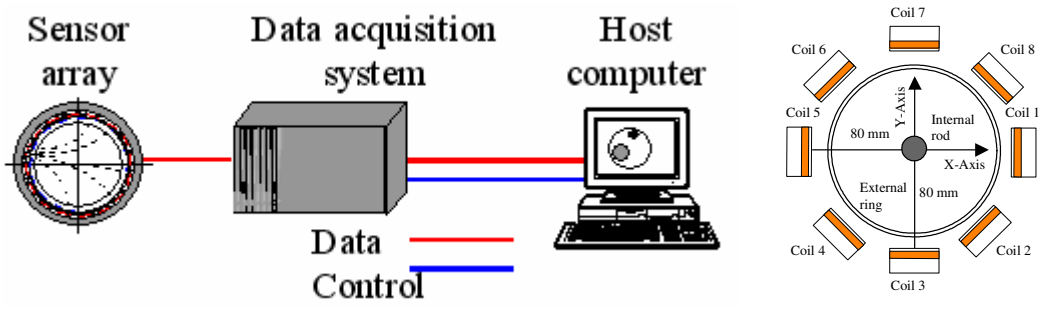

Fig. 1: Block diagram of data acquisition system and 8-coil sensor array, with the object space

B. Continuous casting

Continuous casting, see figure 2, is a key process by which molten steel is formed into semi- finished billets, blooms and slabs. Liquid steel from basic oxygen steelmaking (BOS) or electric arc furnace (EAF) processes and subsequent secondary steelmaking is

transferred from a ladle, via a refractory shroud, into the tundish. The tundish acts as a reservoir, both for liquid steel delivery and removal of oxide inclusions. A stopper rod or sliding gate liquid (not shown) is used to control the steel flow rate into the mould through a submerged entry nozzle (SEN). The SEN distributes the steel within the mould, shrouds the liquid steel from the surrounding environment, and reduces air entrainment thus preventing re-oxidation, and maintaining steel cleanliness. Primary solidification takes place in the water-cooled copper mould and casting powder is used on the surface to protect against re-oxidation and serve as a lubricant in the passage of the strand through the mould. Exiting the mould, the strand consists of a solid outer shell surrounding a liquid core.

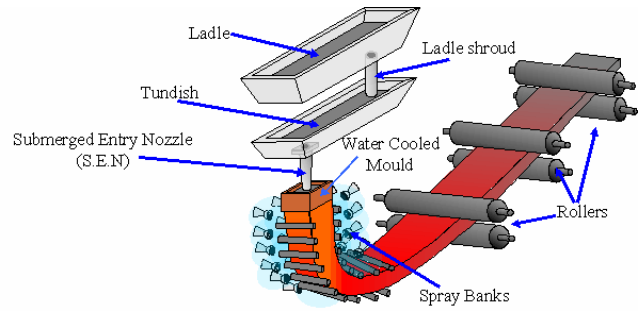

Fig. 2: Continuous casting and SEN

C Experimental test:

Here we use MIT data from a continuous citing unit. Four frames of data were used and their correspondent MIT images were generated using static method as presented in our previous study [11]. Fig. 3 shows the movement of the actual flow and the movement of the metal flow. This shows that the MIT can generate an image that is roughly following the flow pattern. It is important to notice that for more accurate flow images using MIT, one need to use more sensors as well as multiple frequency system. The static

image reconstruction doesn't take into account any correlation between four frames of the MIT images. For the rest of this paper we present a comparison between our new dynamic image methods with the static method. We believe that use of the correlation between multiple image frames will make the dynamical method more reliable. We add noise to already noisy measured data and compare the performance of two methods.

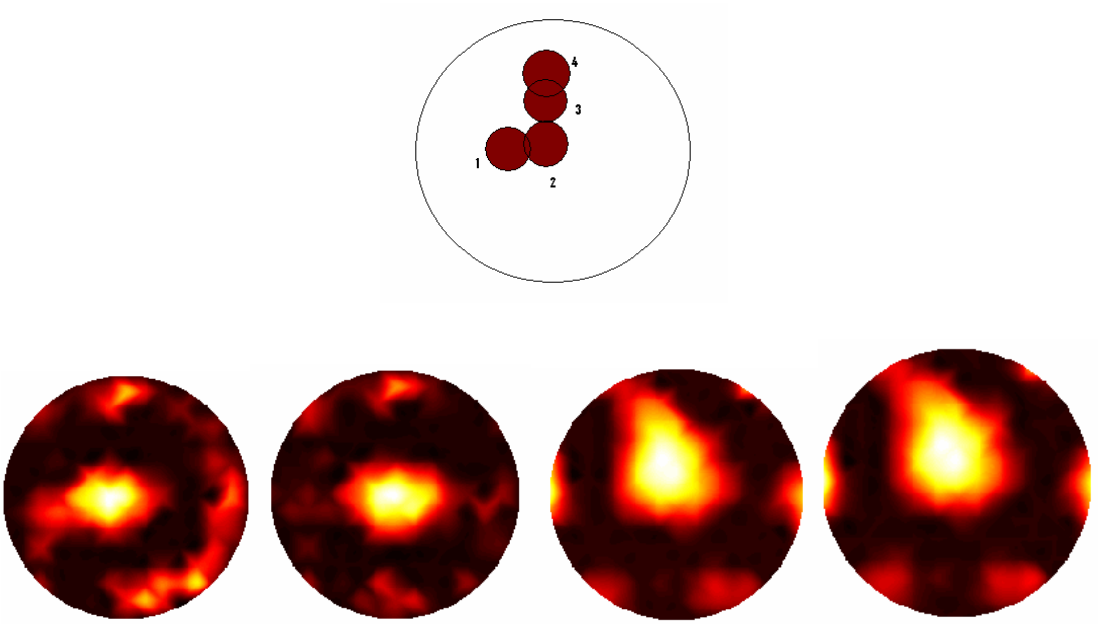

Fig. 3: Four location of the actual flow in SEN and their corresponding static image

The new temporal algorithm was compared to the original GN method with different noise to signal ration (NSR). Different noise levels of NSR=0, 0.1, 0.2, 0.4 were tested. It is worth noticing that NSR=0 is actually the noisy measured data presented in [11], more noise was added to this data to hypothetically generate higher noise level so that the new temporal method compares could be compared with the existing static method. Same regularisation parameter was used for both methods 1e-4; for high noise, 1e-3). The regularization matrix is an identity matrix. Temporal step is set to 1, so that only frame 2, 3, 4 and 5 are reconstructed by using temporal solver because the data set has only 6 frames. Temporal weight is chosen to be 0.8 heuristically, although it might have better

choice. Fig. 3 shows the NRS=0, where two methods are producing similar results. Fig 4, 5,6 shows the comparison between static method and new temporal method with increasing noise level. It can be seen that the reconstructed images by using temporal method are able to produce images closer to NRS=0 than the GN static method, especially for higher noise level. In order to quantatively compare the performance of two methods we define a measure of the image artefact of $im\_err = norm(x - x\_b)/norm(x\_b)$, where x is the image of the given error level and x_b corresponding static image for the case of noise free data (images of figure 3). Table 1 present the image error for various noise levels. As it can be seen visually from higher noise images, the image artifact value is always higher using static method, meaning that the proposed dynamic method could work better in present of higher level of noise.

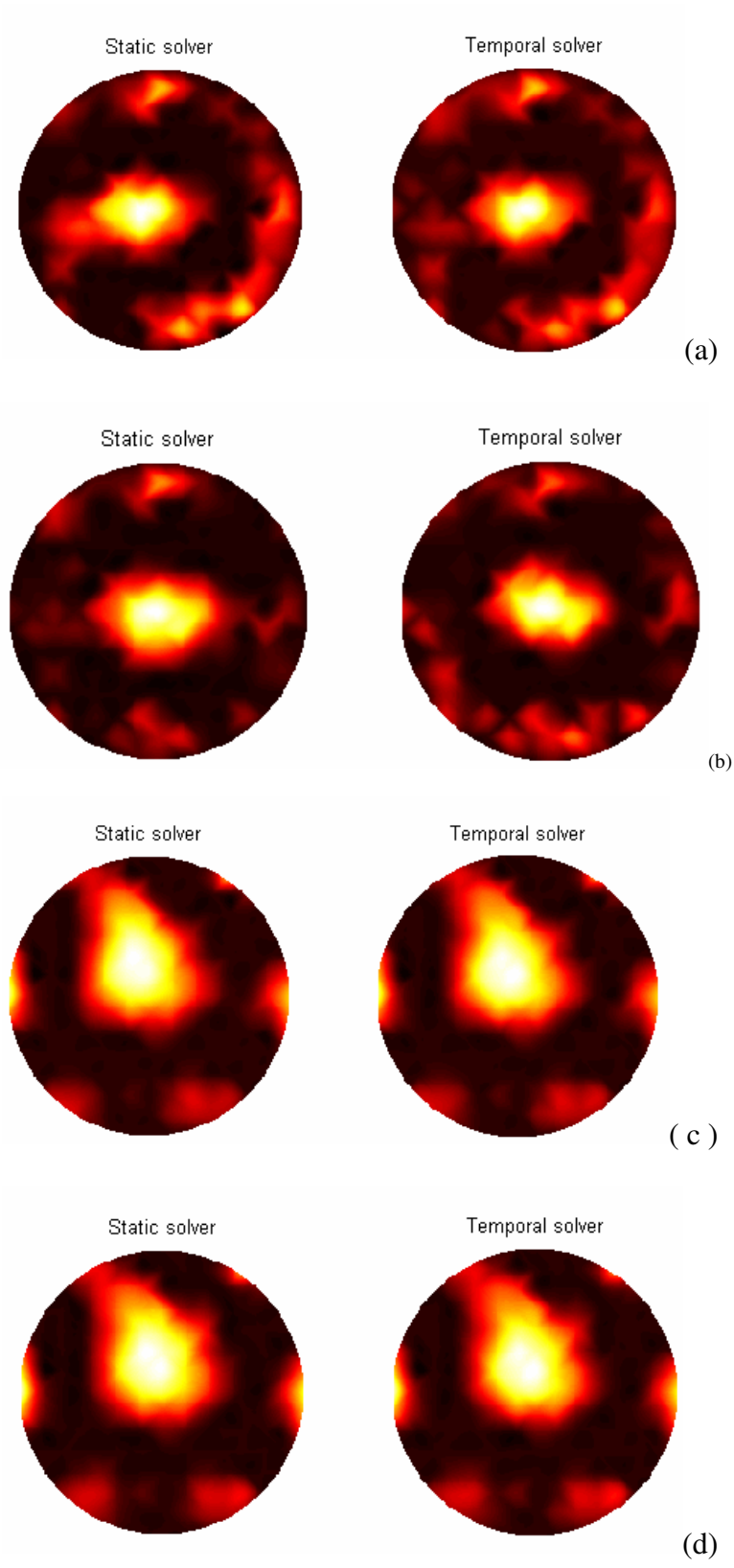

Fig. 4. NSR=0 ; λ =0.0001 ;temporal step is 1 ; temporal weight is 0.8 (left: GN; right: Temporal solver)

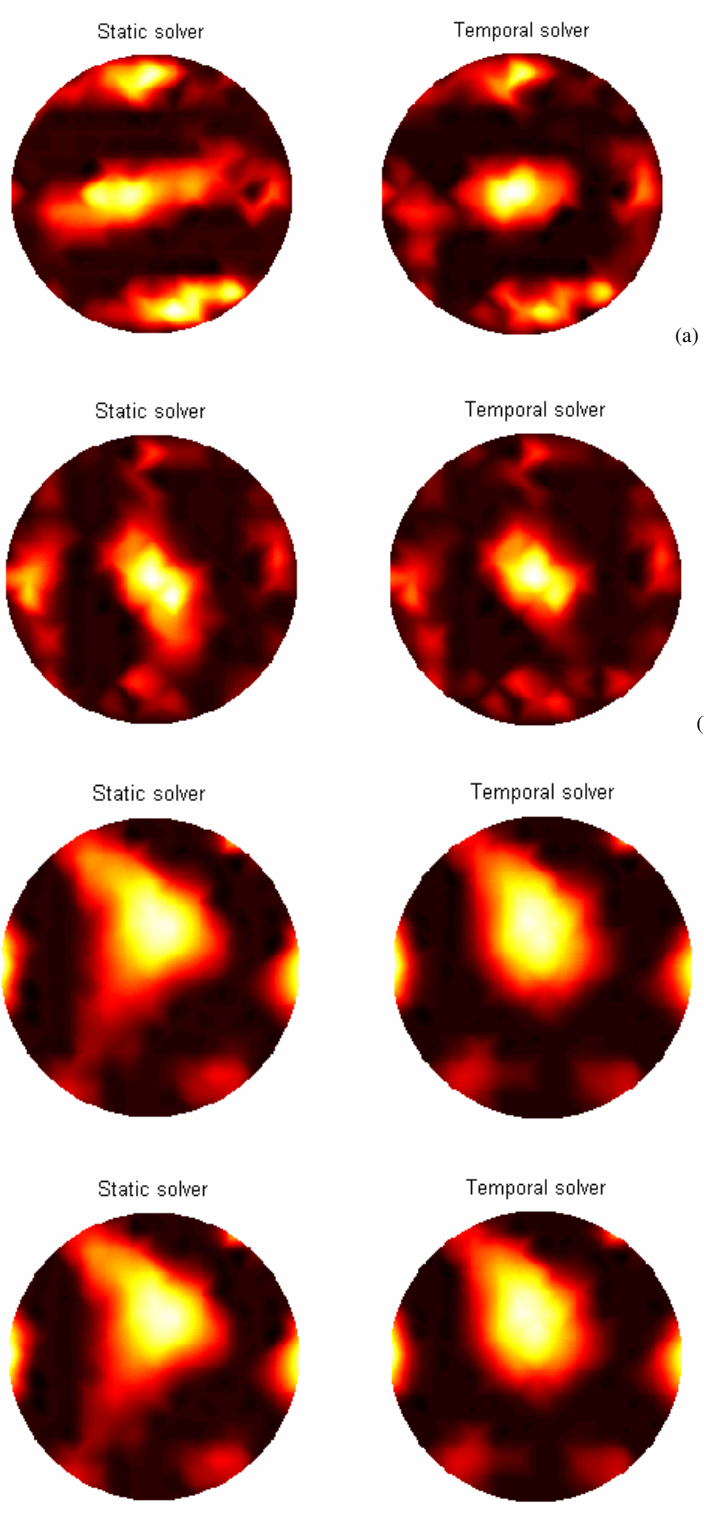

Fig. 5. NSR=0.1 ; λ =0.0001 ;temporal step is 1 ;temporal weight is 0.8 (left: GN; right: Temporal solver)

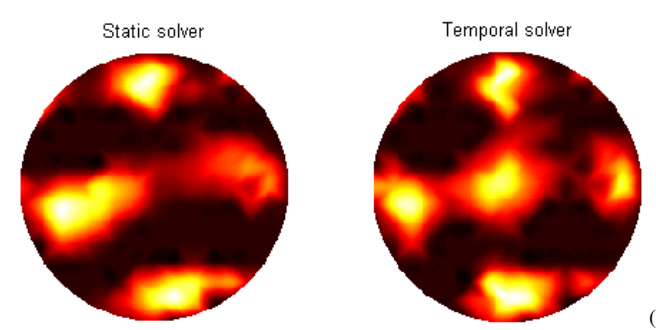

(a)

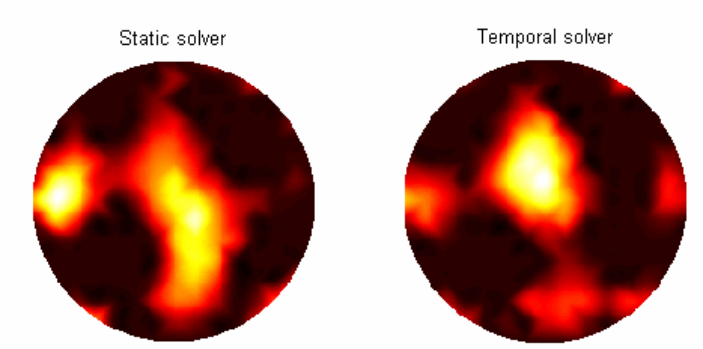

(b)

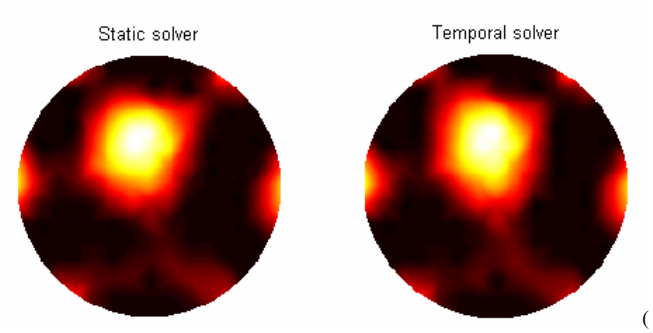

(c)

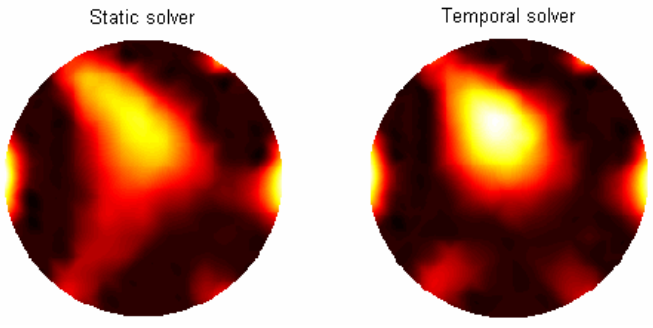

(d)

Fig. 6.NSR=0.2 ; λ =0.001 ;temporal step is 1 ;temporal weight is 0.8 (left: GN; right: Temporal solver)

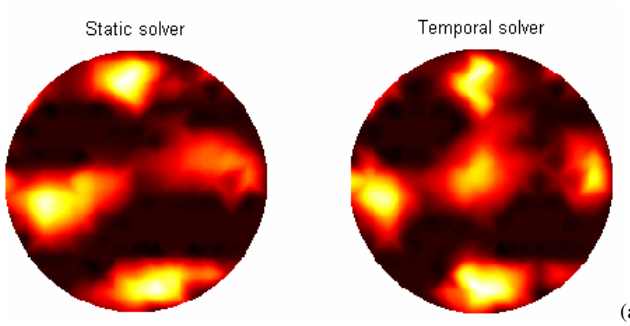

(a)

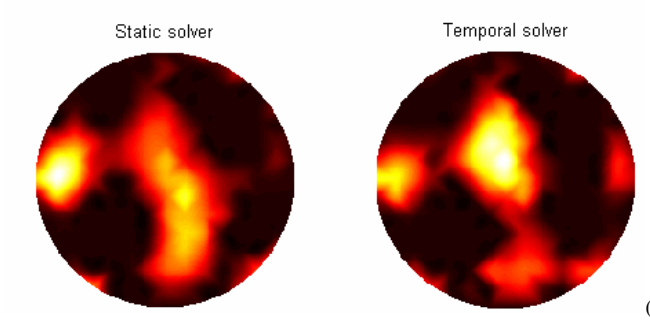

(b)

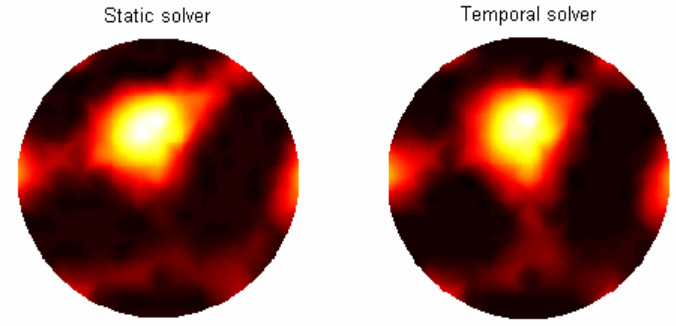

(c)

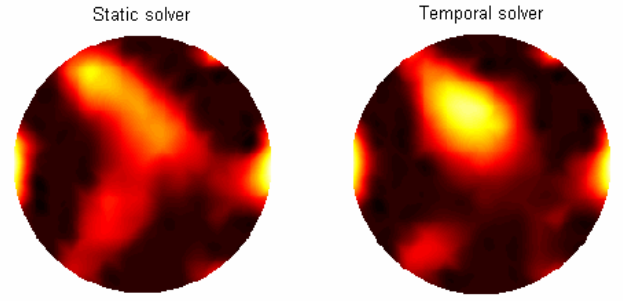

(d)

Fig. 7. NSR=0.4 ; λ =0.001 ;temporal step is 1 ;temporal weight is 0.8 (left: GN; right: Temporal solver)

Table 1: Measure of artefact (*im_err*) for different noise levels

NSR	Frame 1		Frame 2		Frame 3		Frame 4	
	GN	Temp.	GN	Temp.	GN	Temp.	GN	Temp.
0.1	1.2507	0.9734	0.9945	0.7608	0.3694	0.2840	0.3417	0.1753
0.2	1.0657	0.8089	1.2356	0.9705	0.3549	0.3201	0.4059	0.2995
0.4	1.9863	1.6124	2.1400	1.7553	0.6029	0.5200	0.6666	0.5033

4 CONCLUSIONS

In this study, the inverse problem of MIT was treated as a dynamical problem, and the state (conductivity distribution). Dynamic magnetic imaging of a molten metal flow was estimated with the aid of direct temporal imaging method. Temporal solver can achieve better resolution than conventional GN method especially for high noise cases.

The temporal solver could be implemented in MIT applications and it would have faster convergence, or make multi-objects become differentiable at earlier step. The inter-frame image correlation method enables us to generate images that are a psudo-continuous conductivity map.

REFERENCES

1. R. Binns, A. R. A. Lyons, A. J. Peyton, and W. D. N. Pritchard, *"Imaging molten steel flow profiles*," Meas. Sci. Technol., vol. 12, pp. 1132-1138, 2001.
2. D. N. Dyck, D. A. Lowther, and E. M. Freeman, *" A Method of computing the sensitivity of the electromagnetic quantities to changes in the material and sources*," IEEE Trans. Magn., vol. 3, no. 5, pp. 3415-3418, Sep. 1994.

3. H. Griffiths, *"Magnetic induction tomography*," Meas. Sci. Technol., vol. 12, no. 8, pp. 1126-1131, 2001.
4. A Gelb, *" Applied Optimal Estimation*," (Massachusetts: The M.I.T. Press), 1974.
5. MS Grewal and A P Andrews, *"Kalman Filtering: Theory and Practice, Using MATLAB*," (New York: John Wiley & Sons. Inc.), 2001.
6. KY Kim, BS Kim, MC Kim, YJ Lee and M Vauhkonen, *"Image reconstruction in time-varying electrical impedance tomography based on the extended Kalman filter,*" Meas. Scie. Technol, 12, 1032–9, 2001.
7. BS Kim, K Y Kim, T-J Kao, JC Newell, D Isaacson and GJ Saulnier, *"Dynamic electrical impedance imaging of a chest phantom using the Kalman filter*," Physio. Meas., 27 S81–91, 2006.
8. M Soleimani , *Sensitivity maps in three-dimensional magnetic induction tomography*, Insight, Non-Destructive Testing and Condition Monitoring, 48 (1), pp 39-44, 2006
9. X Ma, AJ Peyton, S R Higson, A Lyons and SJ Dickinson**,** Hardware and software design for an electromagnetic induction tomography (EMT) system for high contrast metal process applications**,** *Meas. Sci. Technol.* 17**,** pp 111-118, 2006
10. AJ Peyton, Z Z Yu, S. Al-Zeibak, N H Saunders, and A R. Borges, *"Electromagnetic imaging using mutal inductance tomography: Potential for process applications*," Part. Part. Syst. Charact., vol. 12, pp. 68-74, 1995.

11. M Soleiman, WRB Lionheart, AJ Peyton, X Ma and S Higson, A 3D inverse finite element method applied to the experimental eddy current imaging data, *IEEE Trans Magnetics*, 42 (5), pp 1560-1567, 2006.
12. M. Soleimani, and W.R.B. Lionheart, *"Image reconstruction in three dimensional magnetostatic permeability tomography,*", IEEE Trans.Magn., vol. 41, no. 4, pp. 274-1279, Apr. 2005.
13. M. Soleimani, *"Image and shape Reconstruction for Magnetic Induction and electrical impedance tomography*," PhD thesis, The University of Manchester, 2006.
14. A Adler, T Dai and W R B Lionheart,"*Temporal image reconstruction in electrical impedance tomography*", Physiol. Meas., vol. 28, pp. S1-S11, 2007
15. M Vauhkonen, PA Karjalainen and JP Kaipio, *" A Kalman filter approach to track fast impedance changes in electrical impedance tomography,*" IEEE Trans. Biomed. Eng., 45 486–93, 1998.